Available online at www.sciencedirect.com
SCIENCE DIRECT®
Optics & Laser Technology 35 (2003) 223–232
Optics & Laser Technology
www.elsevier.com/locate/optlastec

A subfringe integration method for multiple-beam Fizeau fringe analysis

M.A. El-Morsy*, K. Harada, M. Itoh, T. Yatagai

Yatagai Laboratory, Institute of Applied Physics, University of Tsukuba, Tsukuba, Ibaraki 305-5873, Japan

Received 22 March 2002; received in revised form 29 November 2002; accepted 4 December 2002

Abstract

Some aspects concerning the subfringe integration method in interferogram analysis have been investigated and modified. The modified algorithm, introduced in this paper, is capable of reconstructing the phase in the presence of noise or errors in carrier frequency. The subfringe integration method was applied to analyze two computer simulated patterns of equispaced Fizeau fringes using N bucket integration. Also, it is used to analyze the multiple-beam Fizeau fringe. The refractive index profile of polyethylene fiber is obtained by using two methods, subfringe integration method, and Fourier transform method. A comparison between the obtained results using the maintained methods is presented.

Keywords: Automatic fringe analysis; Subfringe integration; Fourier transform; Phase measurement; Multiple beam Fizeau fringes; Refractive index profile; Polyethylene fiber

1. Introduction

Because of the determination of the phase difference in interferometry is directed to the physical quantity to be measured, the last three decades have seen an upsurge of interest in optical interferometric measurement. Phase measurement interferometry is the most widely used technique to directly measure wavefront phase in an interferometer corresponding to the relative difference between the test and reference optical paths. The direct measurement of phase information has many advantages over simply recording interferogram and digitizing the position of the fringe maxima and minima. The main advantages of optical interferometric measurement are the two-dimensional phase that can be measured with high precision and automated by fast measurement using computer-aid.

The phase-shifting method is an effective technique for fringe analysis to obtain the phase distribution. In this case the phase difference between the two interfering beams mutate in a known manner [1]. We acquire the phase value by calculating the intensity change of an investigated point corresponding to at least three different phase shifts.

There are many different methods to introduce phase shift or modulation in an interferometer [2,3], for example moving a mirror, tilting a glass plate, moving a grating and rotating a half-wave plate or analyzer. A simple and a common straightforward way to introduce phase shifting technique is to mount one of the mirrors of the interferometer on a piezoelectric transducer (PZT) and apply a suitable voltage to the PZT. Many brands of PZT are available to linearly move a mirror over many micrometers. Accurate calibration of the PZT is then very important to obtain the desired phase shifts between data frames.

The fringe pattern analysis techniques provide a powerful tool in optical interferometric measurement for accurate determination of phase. Numerous authors used interferometric pattern to determine the phase of an unknown wavefront. Each has proposed a phase extraction algorithm appropriate for his particular data-acquisition scheme [4].

There are many different techniques for quantitative phase measurement from fringe patterns. These techniques can be classified into two categories: temporal [5] and spatial [6] techniques. Temporal technique takes the phase data sequentially while spatial technique takes the phase data simultaneously. Each of the techniques has its own fundamental advantages and disadvantages in accuracy, range of measurement, and type of object that can be measured.

* Corresponding author. Fax: +81-298-535-205.
E-mail address: elmorsym@yahoo.com (M.A. El-Morsy).

0030-3992/03/$ - see front matter © 2003 Elsevier Science Ltd. All rights reserved.
doi:10.1016/S0030-3992(02)00177-9

The oldest and the simplest method used for the fringe pattern analysis supported by image processing is the fringe tracing method. With this technique it is possible to evaluate the phase modulation with one image only and in a wide range of values [7]. The main advantage of this technique is that there is no phase unwrapping, but this technique has the disadvantage of having a high sensitivity to noise, compared with other techniques such as Fourier transform.

Fourier transform technique of fringe pattern analysis is useful in removing the noise from the fringe pattern. Fourier fringe analysis was originally introduced and demonstrated by Takeda et al. [8,9]. The technique has also been studied by many others [10–14]. The major advantage of this technique is that it usually requires only one interference fringe pattern for extracting phase information; moreover, the higher harmonics can be removed in computation. The main disadvantage of this technique is the processing of transform, filtering and inverse transform take a long time; furthermore, the automatic selection of filtering windows in spectrum domain is very difficult especially if there is overlap between the peaks [15].

From the point of view of accuracy, the best technique used for evaluating the phase distribution is the subfringe integration algorithm. This technique has the advantage of having a high resistance to noise and to error due to errors in carrier frequency. Furthermore, it does not need phase shifting devices because it uses only one fringe pattern.

In this paper we will investigate and modify the subfringe integration method in order to reduce the effect of noise and the error due to errors in carrier frequency. Moreover, we used it to analyze the multiple-beam Fizeau fringes.

2. Explanation of the subfringe technique for a fringe analysis

Let us first describe the basic principle of the subfringe technique. The intensity distribution of linear and equispaced Fizeau fringes can be written as

$$I(x) = a(x)\left[1 + b(x)\cos\left(\frac{2\pi x}{T} + \Phi(x)\right)\right], \quad (1)$$

where $a(x)$ represents the background illumination of the intensity distribution $I(x)$, $b(x)$ describes the amplitude of the corresponding interference fringe, T is the fringe period, $\Phi(x)$ is the phase of the object that we have to analyze at any point (x) on the interferogram.

The main idea of integration method is that the period of the sinusoidal signal is divided into at least three or more buckets and integrates each bucket. The whole integration analysis method process is illustrated in Fig. 1. Wyant

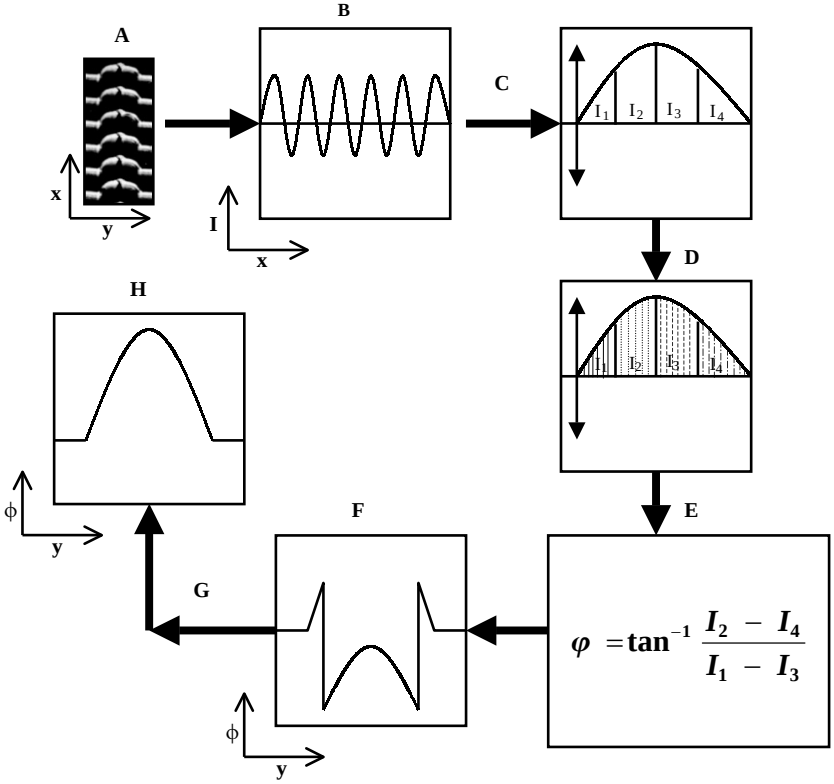

Fig. 1. Integration analysis method process: (A) original pattern; (B) 1-D intensity distribution; (C) dividing the fringe period into four buckets; (D) integration of each bucket process; (E) calculating the phase; (F) wrapped phase obtained; (G) unwrapped process; (H) unwrapped phase obtained.

used four integrating buckets in the temporal domain [16]. Recently, Wang et al. used four integrating buckets in the spatial domain [17]. Wang et al. described the four-intensity integration bucket over a finite space as

$$I = \int_{-T/8}^{T/8} I(x)\,\mathrm{d}x + \int_{T/8}^{3T/8} I(x)\,\mathrm{d}x + \int_{3T/8}^{5T/8} I(x)\,\mathrm{d}x + \int_{5T/8}^{7T/8} I(x)\,\mathrm{d}x = I_1 + I_2 + I_3 + I_4 \tag{2}$$

in this case, the phase is given by

$$\varphi = \tan^{-1}\left(\frac{I_4 - I_2}{I_1 - I_3}\right). \tag{3}$$

According to the limits of integration we need to shift the origin of the signal by $T/8$. But for more accuracy, we changed this limits of integration to be $(0, T/4)$, $(T/4, T/2)$, $(T/2, 3T/4)$, $(3T/4, T)$. In this case we do not need to shift the origin of the signal. Eq. (2) becomes

$$I = \int_{0}^{T/4} I(x)\,\mathrm{d}x + \int_{T/4}^{T/2} I(x)\,\mathrm{d}x + \int_{T/2}^{3T/4} I(x)\,\mathrm{d}x + \int_{3T/4}^{T} I(x)\,\mathrm{d}x = I_1 + I_2 + I_3 + I_4, \tag{4}$$

where

$$I_1 = A + B[\cos\Phi - \sin\Phi],$$

$$I_2 = A + B[-\cos\Phi - \sin\Phi],$$

$$I_3 = A + B[-\cos\Phi + \sin\Phi], \tag{5}$$

$$I_4 = A + B[\cos\Phi + \sin\Phi],$$

and

$$A = \frac{T}{4}\,a(x), \qquad B = \frac{T}{2\pi}\,b(x).$$

The phase is retrieved by applying the equation

$$\Phi = \tan^{-1}\left(\frac{(I_1 + I_2) - (I_3 + I_4)}{2(I_2 - I_1)}\right) \tag{6}$$

by the same way the phase, in case five, six, seven, eight buckets, can rewritten as the following equation, respectively:

$$\Phi_{5\ \text{buckets}} = \tan^{-1}\left(\frac{(I_3 + I_4) - (I_1 + I_2)}{(I_5 - I_2) + (I_1 - I_2)}\right),$$

$$\Phi_{6\ \text{buckets}} = \tan^{-1}\left(\frac{(I_3 + I_4) - (I_1 + I_2)}{(I_5 - I_6) + (I_1 - I_2)}\right),$$

$$\Phi_{7\ \text{buckets}} = \tan^{-1}\left(\frac{(I_3 + I_4) - (I_1 + I_2) + (I_7 - I_6)}{(I_5 - I_6) + 2(I_1 - I_2)}\right),$$

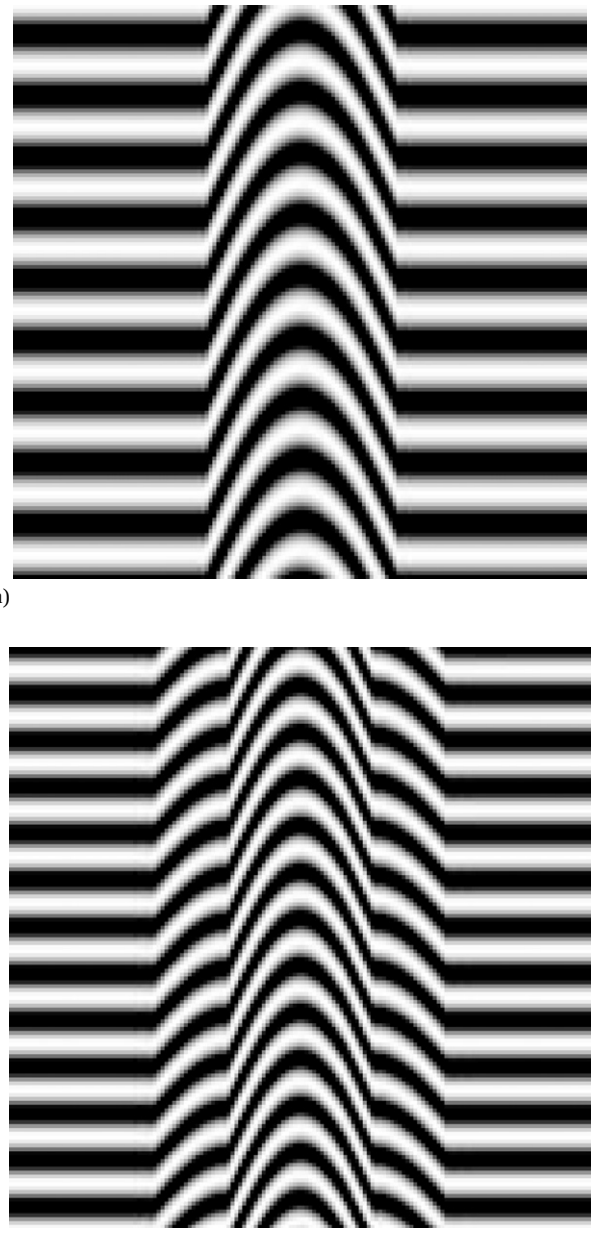

(a)

(b)

Fig. 2. Two computer-simulated interferogram of equispaced Fizeau fringes.

$$\Phi_{8\ \text{buckets}} = \tan^{-1}\left(\frac{((I_3 + I_4) - (I_1 + I_2)) + ((I_8 + I_7) - (I_5 + I_6))}{2(I_5 - I_6) + 2(I_1 - I_2)}\right). \tag{7}$$

In most phase-measurement techniques, the phase unwrapping is an inevitable consequence because of the nature of the function used to calculate the phase values lie between $\pm\pi$ radians or between 0 and 2π. In other words the arctan function provides only principle values of the phase. These principle values are called wrapped phase values because

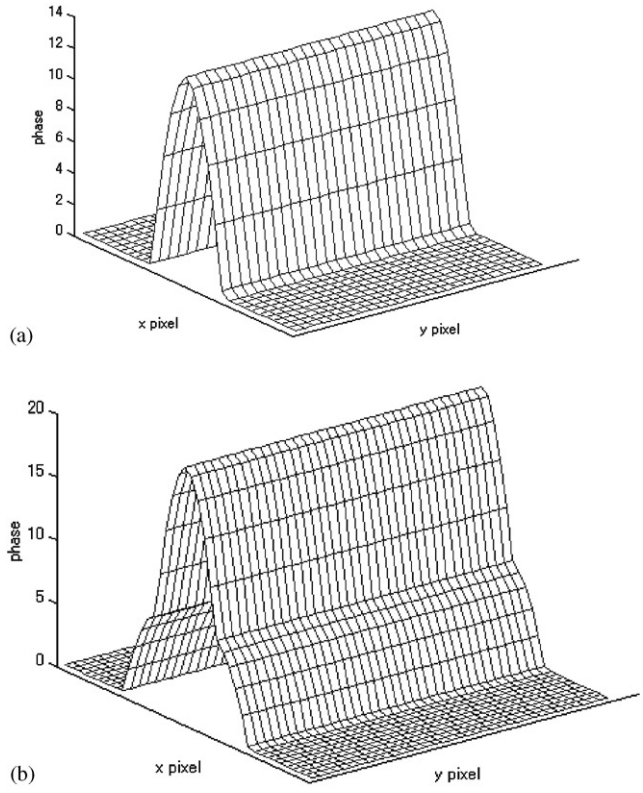

Fig. 3. Two-dimensional (2D) unwrapped continuous phase distribution (a) using interferogram 2a, (b) using interferogram 2b.

the absolute phase is wrapped into interval $(-\pi, \pi]$ [7]. So phase ambiguities must then be removed using a phase unwrapping techniques. In addition, the carrier frequency tilt fringes will result in a large tilt of the measured phase. The tilt due to the carrier fringes then need to be subtracted in order to obtain the original phase. There are many techniques for unwrapping phase. In this work we used two simplest techniques. The first one is the algorithm, which was used by Takeda [8] and the other named Itoh technique [18]. In fact we observed that the two techniques give essentially the same final unwrapped phase.

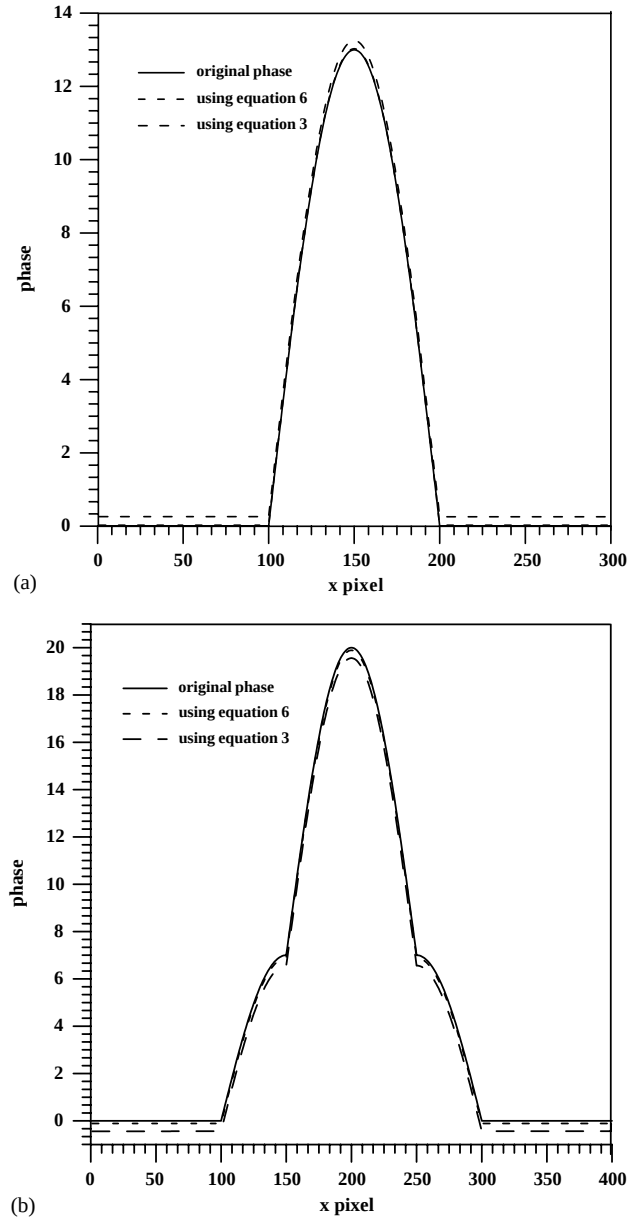

Fig. 4. The original and the reconstructed unwrapped phase calculated using Eqs. (3) and (6): (a) using interferogram 2a, (b) using interferogram 2b.

3. Results of computer simulation

3.1. Noise-free interferogram

The subfringe method was tested by using two different computer-simulated of equispaced Fizeau fringes, in case of using a matching and mismatching immersion liquids, shown in Figs. 2a and b, respectively. The obtained phase after processing the interferogram (Fig. 2) using subfringe method is shown in Figs. 3a and b. Fig. 4 shows a comparison of the reconstructed phase using Eqs. (3) and (6). From Fig. 4 it is clear that the reconstructed phase using Eq. (6) is more accurate than the reconstructed phase in case of using Eq. (3). For example in Fig. 4a, the average deviation of the reconstructed phase from the original phase is 1.56134×10^{-4} which calculated using Eq. (6) corresponding to 1.48404×10^{-3} in case of using Eq. (3).

3.2. Noise interferogram

There is no doubt that one of the biggest problems involved in practical digital fringe pattern analysis is the noise reduction problem, regardless of the type of image processing method used. Without noise the fringe pattern analysis

becomes much easier to be analyzed and is usually straightforward. But unfortunately, during the acquisition and digitization of the fringe pattern various noises appear in the digital fringe patterns [19]. Introducing noise function due to detector error, Eq. (1) can be rewritten as

$$I(x) = a(x)\left[1 + b(x)\cos\left(\frac{2\pi x}{T} + \varphi(x)\right) + n(x)\right], \qquad (8)$$

where $n(x)$ is the noise distribution function, which influences both the bias and the visibility of the fringe pattern, and given by

$$n(x) = \delta\,\mathrm{random}(x),$$

where δ is the parameter of noise and random(x) is random number between the interval (0, 1). We created this random number by using MATALB function rand(x) which

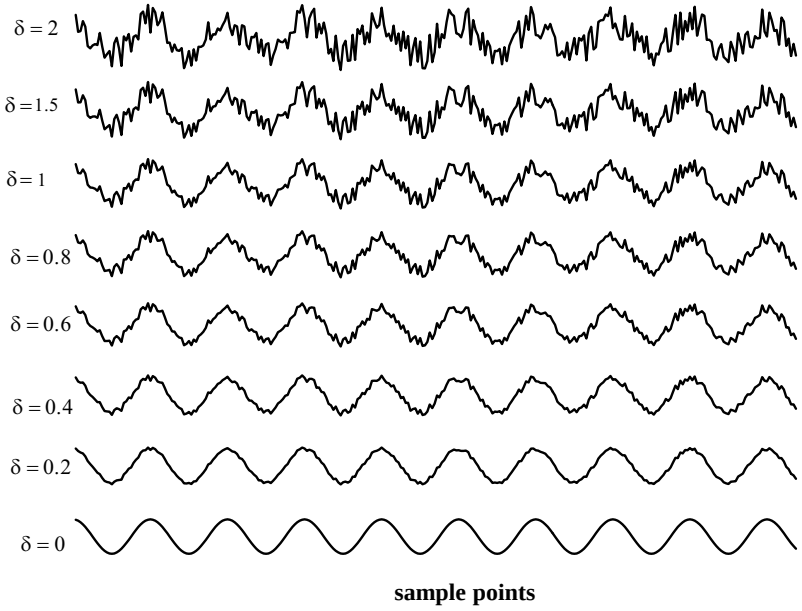

Fig. 5. An example of intensity of 1D fringe pattern with different parameter of noise δ.

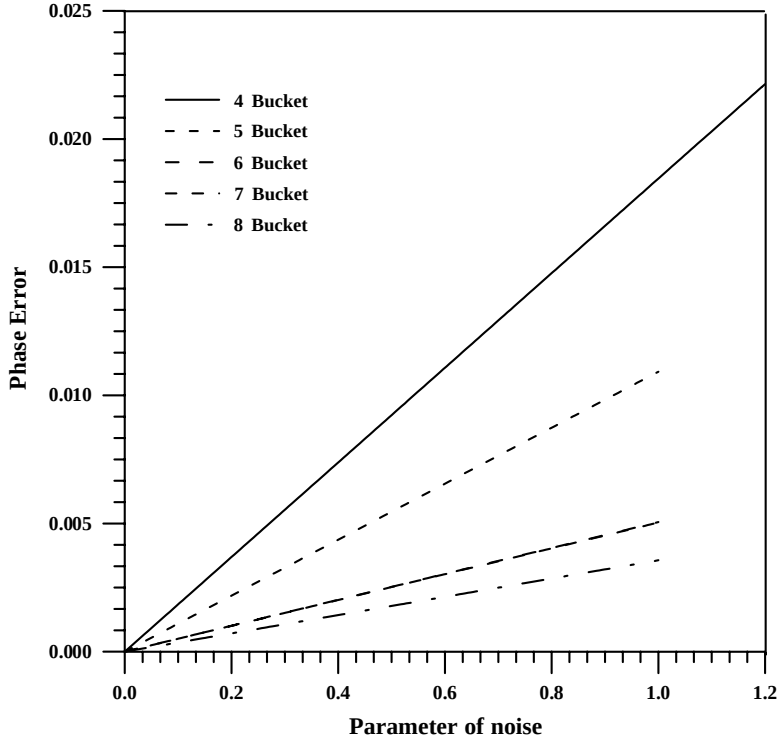

Fig. 6. The average deviation of the reconstructed phase from the original phase versus the parameter of noise, with different bucket number.

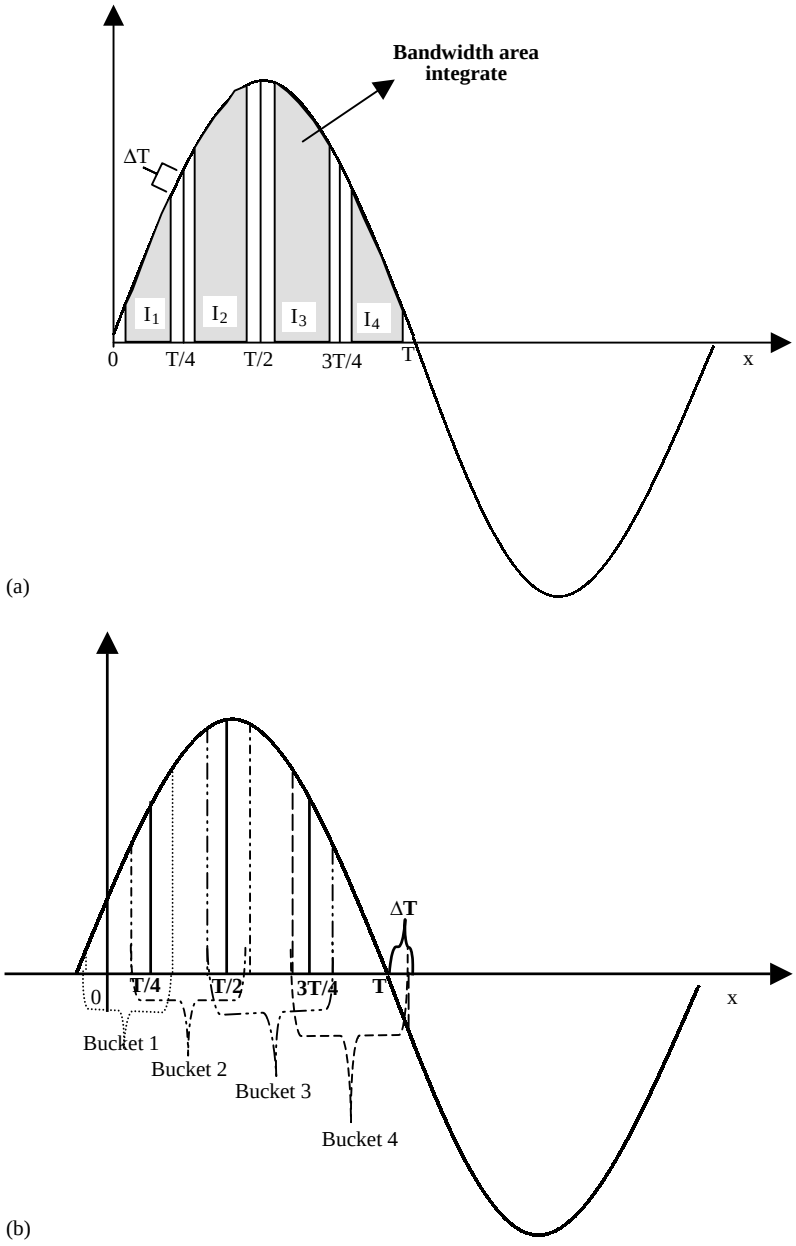

Fig. 7. Four buckets integrating in subfringe integrating method: (a) bandwidth integrate, (b) overlap integrate.

produce uniformly distributed random numbers and arrays. Fig. 5 shows the intensity distribution with different noise parameter (δ). There is no doubt that the larger noise parameter the larger average deviation of the reconstructed phase from the original phase. To reduce the average deviation of the reconstructed phase from the original phase we used the subfringe integration method with four, five, six, seven, and eight buckets. Curve 1 in Fig. 6 shows the average deviation of the reconstructed phase from the original phase using four buckets while curve 2, 3, 4, and 5 have been obtained by using five, six, seven and eight buckets respectively. From the average deviation curves shown in Fig. 6 it is clear that the more buckets the smaller average deviation.

4. Reduce the effects of major fundamentals errors

In practice, the accuracy in the phase measurement calculation is affected by a variety of events, such as wrong carrier frequency, noise, unequally spaced fringes, detector non-linearities, and variations in the dc fringe intensity. Creath and Schmit discussed in detail N-point spatial phase-measurement technique error [20]. So in the following analysis we will neglect to discuss all the error effects but we will discuss only how to reduce the effect of noise and wrong carrier frequency with the integration method. Phase measurements of higher precision can be done with variation of the limits of integration of the buckets by two

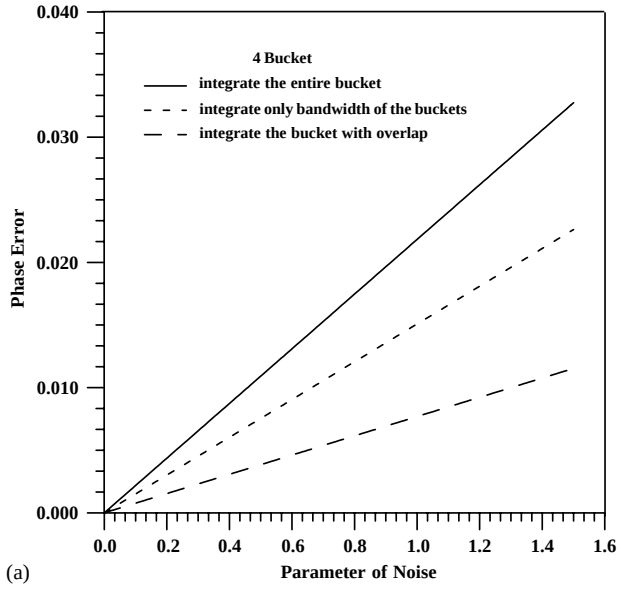

(a)

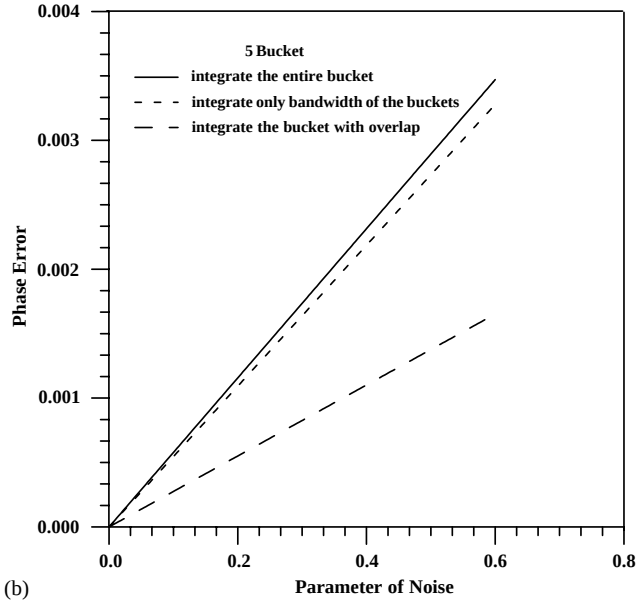

(b)

Fig. 8. Average deviation of the reconstructed phase from the original phase versus the parameter of noise, with different bucket area integrate: (A) using four buckets, (b) using five buckets.

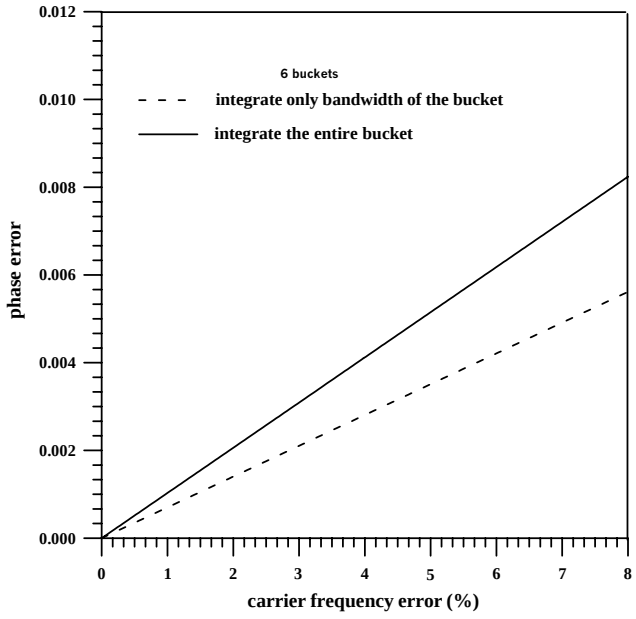

Fig. 9. The average deviation of the reconstructed phase from the original phase versus the carrier frequency error, with different bucket area integrate, using six buckets.

Table 1
Statistical comparisons between the average deviation of the reconstructed phase from the original phase in case integrate the entire of the buckets and integrate only bandwidth of the buckets, when using seven buckets

Carrier frequency error (%)	Average deviation	
	Integrate the entire of the buckets	Integrate only bandwidth of the buckets
2	8.97×10^{-4}	8.97×10^{-4}
4	6.44×10^{-4}	1.3×10^{-3}
6	4.5×10^{-3}	1.3×10^{-3}
8	5.3×10^{-3}	3.4×10^{-3}
10	9.1×10^{-3}	6.3×10^{-3}
15	12×10^{-3}	11.9×10^{-3}
20	35.3×10^{-3}	18.9×10^{-3}

methods. The first method is not to integrate the entire bucket but integrate bandwidth in the bucket (bandwidth integrate). For example, the limit of first bucket changes from $(0, T/4)$ to $(0 + \Delta T, T/4 - \Delta T)$ as shown in Fig. 7a. In the second method, the limits of integration change provided that there is an overlap between the buckets with each other (integrate with overlap). In other words, the limits of integrate first bucket become from $(0, T/4)$ to $(0-\Delta T, T/4+\Delta T)$ as shown in Fig. 7b. Fig. 8 presents a comparison of the average deviation of the reconstructed phase from the original phase as a function of the parameter of noise with the proposed methods. Fig. 8a has been obtained by using Four buckets while Fig. 8b has been obtained using five buckets. It is seen that using the proposed methods we can avoid the divergence of the reconstructed phase from the original phase in the presence of noise. We are essentially able to reduce the effect of wrong carrier frequency using the bandwidth integrate method as shown in Fig. 9. Table 1 gives the average deviation of the reconstructed phase from the original phase obtained from seven buckets when using the bandwidth integrate method.

5. Experimental results

The refractive index profile, shape and value plays an important role in characterizing the natural, synthetic

and optical fiber because of several major advances in its related technologies. The refractive index profile measurement using multiple-beam Fizeau interference of the Fizeau technique gives accurate results due to the sharpness of the interference fringe compared with two-beam interference [21]. Therefore, many authors used the multiple-beam Fizeau interference technique to measure the refractive index profile to textile and optical fibers [22–25].

In the multiple-beam Fizeau interference technique the fiber samples are immersed in a silvered liquid wedge interferometer. In this case the fiber acts as phase objects displacing the normally straight parallel fringes to the fiber region. This fringe displacement is proportional to the refractive index of the fiber. Considering the refraction of the beam through the fiber due to the refractive index change along its radius and the cross section of the fiber divided into large number of layers, Q, each of them is considered to have a constant refractive index; the equation used to calculate the refractive index profile of the fiber is given by [26]

$$\frac{\lambda\phi_Q}{4\pi}=\left[\begin{array}{l}\displaystyle\sum_{j=1}^{Q-1}2n_j\left\{\begin{array}{l}\sqrt{(R-(j-1)a)^2-(d_Qn_o/n_j)^2}\\ -\sqrt{(R-ja)^2-(d_Qn_o/n_j)^2}\end{array}\right\}\\ \quad+2n_Q\sqrt{(R-(Q-1)a)^2-(d_Qn_o/n_j)^2}\\ \quad-n_o\{\sqrt{R^2-d_Q^2}+\sqrt{R^2-X_Q^2}\}\end{array}\right], \tag{9}$$

where λ is the wavelength of light used, R is the fibre radius, a is the layer thickness ($a = R/Q$), $n_o = n_L$ is the immersion liquid refractive index, X_Q and d_Q are the emerged and incident rays distances from the fiber center, respectively, where

$$d_Q=\frac{n_Q(R-(Q-\frac{1}{2})a)}{n_o}. \tag{10}$$

And considering the phase difference is given by

$$\phi=\phi(R)-\phi_o,$$

where $\Phi(R)$ is the phase shift due to the fiber and Φ_o is the phase due to the immersion liquid.

Fig. 10 shows the interferogram of multiple-beam transmitted Fizeau fringes when using monochromatic light of wavelength 546.1 nm vibrating parallel to the polyethylene fiber axis and the refractive index of the immersion liquid is 1.5787. We analyzed Fig. 10 using two techniques, subfringe integration method and Fourier transform method, to obtain the phase distribution and the refractive index profile of the fiber. The refractive index profile obtained using both maintained methods is shown in Fig. 11. It is clear that the difference between the refractive index

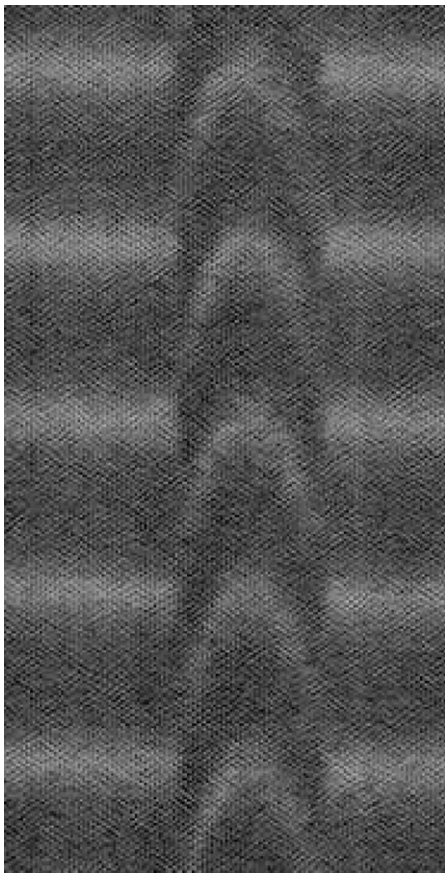

Fig. 10. Microinterferogram of polyethylene fiber using monochromatic light of wavelength 546.1 nm vibrating parallel to the fiber axis, immersion liquid used is 1.5787.

measurement that obtained by the subfringe integration and Fourier transform methods is small and the two curves coincide with each other and tend to be one curve.

6. Conclusions

The subfringe integration method, like Fourier transform method, has a major advantage, such as it requires one only interference fringe pattern and it has a high resistance to noise and to error due to the errors in carrier frequency. Furthermore, it does not need processing of transform, filtering, and inverse transform which take long time in calculation.

The subfringe integration algorithm introduced in this paper is easy to implement, effective in the determination of phase distribution, and have achieved better accuracy in the presence of noise. This technique was tested by using two different computer simulated of equispaced Fizeau fringe. It has shown high-precision evaluation of the phase distribution of multiple-beam Fizeau fringe.

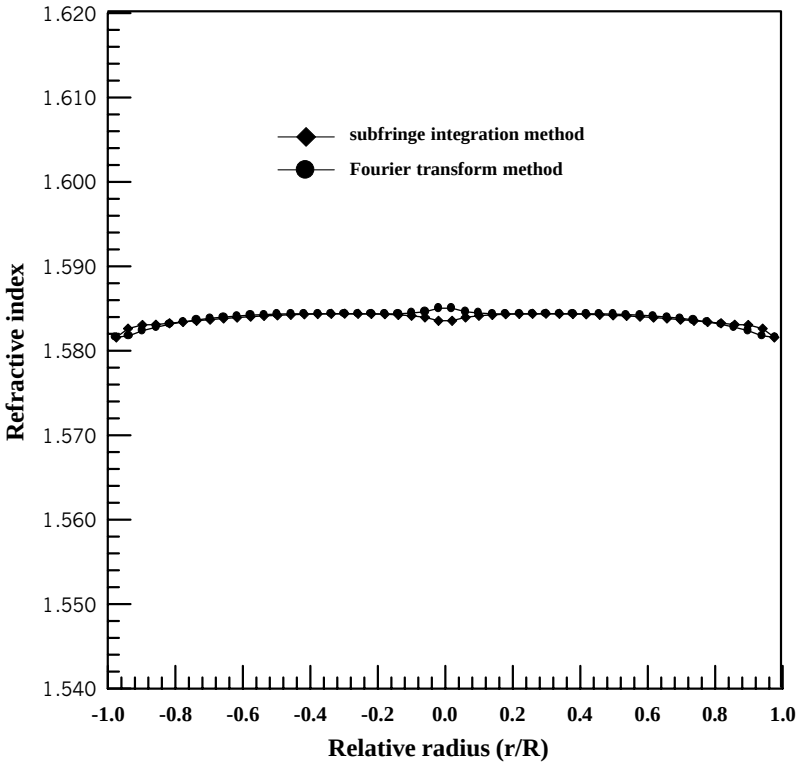

Fig. 11. Refractive index profile of polyethylene fiber using subfringe integration method and Fourier transform method, monochromatic light vibrating parallel to the fiber axis is used and the immersion liquid used is 1.5787.

From the computer simulation and experimental result, we can conclude that the subfringe integration method is a powerful technique to analyze the multiple-beam Fizeau fringe pattern to measure the refractive index profile of polyethylene fiber.

References

[1] Creath K. Phase-measurement interferometry techniques. In: Wolf E, editor. Progress in optics, vol. 26. Amsterdam: North-Holland. 1988 p. 350–93.

[2] Robinson DW, Reid TG. Interferogram analysis. Bristol, Philadelphia: Institute of Physics Publishing, 1993.

[3] Heriharam HP, Oreb FB, Eiju T. Digital phase-shifting interferometry: a simple error-compensating phase calculation algorithm. Appl Opt 1987;26(13):2504–5.

[4] Malacara D, Servin M, Malcara K. Interferogram analysis for optical testing. New York: Marcal Dekker, Inc, 1998.

[5] Creath K. Temporal phase measurement methods. In: Robinson DW, Reid TG, editors. Interferogram analysis. Bristol, Philadelphia: Institute of Physics Publishing, 1993. p. 94–140.

[6] Kujawinsha M. Spatial phase measurement methods. In: Robinson DW, Reid TG, editors. Interferogram analysis. Bristol, Philadelphia: Institute of Physics Publishing, 1993. p. 141–93.

[7] Funnell WRJ. Image processing applied to the interactive analysis of interferometric fringes. Appl Opt 1981;20(18):3245–50.

[8] Takeda M, Ina H, Kobayashi S. Fourier-transform method of fringe-pattern analysis for computer-based topography and interferometry. J Opt Soc Am 1982;72:156–60.

[9] Takeda M, Mutoh K. Fourier transform profilometry for the automatic measurement of 3-D object shapes. Appl Opt 1983;22:3977–82.

[10] Bone DJ. Fourier fringe analysis: the two-dimensional phase unwrapping problem. Appl Opt 1991;30:3627–32.

[11] Nugent KA. Interferogram analysis using an accurate fully automatic algorithm. Appl Opt 1985;24:3101–5.

[12] Lai G, Yatagai T. Use of the fast Fourier transform method for analyzing linear and equispaced Fizeau fringes. Appl Opt 1994;33:5935–40.

[13] Arevalillo M, Burton DR, Lalor MJ. Accelerating fast Fourier transform and filtering operations in Fourier fringe analysis for accurate measurement of three-dimensional surfaces. Opt laser Eng 1999;31:135–45.

[14] Green RJ, Walker JG, Robinson DW. Investigation of the Fourier-transform method of fringe pattern analysis. Opt laser Eng 1988;8:29–44.

[15] Wang M, Ma L, Li D, Zhong J. Subfringe integration method for automatic analysis of moire deflection tomography. Opt Eng 2000;39(10):2726–33.

[16] Wyant CJ. Use of an ac heterodyne lateral shear interferometer with real-time wavefront correction systems. Appl Opt 1975;14(11): 2622–6.

[17] Wang M, Zhong J, Li D. Subfringe integration profilometry of three-dimensional diffuse objects. Opt Eng 1997;36(9):2567–72.

[18] Itoh K. Analysis of the phase unwrapping problem. Appl Opt 1982;21(14):2470.

[19] Hamza AA, Sokkar TZN, Mabrouk MA, El-Morsy MA. Refractive index profile of polyethylene fiber using interactive multiple-beam fizeau fringe analysis. J Appl Polym Sci 2000;77:3099–106.

[20] Creath K, Schmit J. N-point spatial phase measurement techniques for non-destructive testing. Opt Las Eng 1996;24:365–79.

[21] Barakat N, Hamza AA. Interferometry of fibrous materials. Bristol, New York: Adam Hilger, 1990.

[22] Barakat N, Hamza AA, Gonied AS. Multiple-beam interference fringe applied to GRIN optical waveguides to determine fibre characteristics. Appl Opt 1985;24:4383–6.
[23] Hamza AA, Sokkar TZN, Mabrouk MA, Ghandar AM, Ramadan WA. On the determination of the refractive index of a fibre: II graded index fibre. Pure Appl Opt 1995;4:161–77.
[24] Mabrouk MA, Shams-Eldin MA. Interferometric measurement of some structural parameters of drawn Polyethylene fibres. Pure Appl Opt 1996;5:929–40.
[25] Mabrouk MA, El-Bawab HF. Refractive index profile of GR-IN optical fibre considering the area under the interference fringe shift: I. The matching case. Pur Appl Opt 1997;6: 247–56.
[26] El-Morsy AM, Yatagai T, Hamza AA, Mabrouk AM, Sokkar NZT. Automatics refractive index profiling of fibers by phase analysis method using Fourier transform. J Opt Las Eng 2002;38: 509–25.